Absolute measurements of the high-frequency magnetic dynamics in high- T_c superconductors

S.M. Hayden^a, G. Aeppli^b, P. Dai^c, H.A. Mook^c, T.G. Perring^d, S.-W. Cheong^e, Z. Fisk^f, F. Doğan^g, T.E. Mason^h

^aH.H. Wills Physics Laboratory, University of Bristol, Bristol BS8 1TL, UK

^bNEC Research Institute, Princeton, NJ 08540, USA

^cOak Ridge National Laboratory, Oak Ridge, TN 37831, USA

^dRutherford Appleton Laboratory, Chilton, Didcot, OX11 0QX, UK

^eBell Laboratories, Lucent Technologies, NJ 07974, USA

^fDepartment of Physics, Florida State University, Tallahassee, Florida 32306, USA

^gDepartment of Material Science and Engineering, University of Washington, Seattle,

Washington 98195, USA

^hDepartment of Physics, University of Toronto, Toronto, Canada M5S 1A7 (27 August 1997)

Abstract

We review recent measurements of the high-frequency dynamic magnetic susceptibility in the high- T_c superconducting systems $\text{La}_{2-x}\text{Sr}_x\text{CuO}_4$ and $\text{YBa}_2\text{Cu}_3\text{O}_{6+x}$. Experiments were performed using the chopper spectrometers HET and MARI at the ISIS spallation source. We have placed our measurements on an absolute intensity scale, this allows systematic trends to be seen and comparisons with theory to be made. We find that the insulating $S = \frac{1}{2}$ antiferromagnetic parent compounds show a dramatic renormalization of the spin wave intensity. The effect of doping on the response is to cause broadenings in wave vector and large redistributions of spectral weight in the frequency spectrum.

I. INTRODUCTION

The collective excitations of the spins in the CuO₂ planes of the high temperature superconductors display a plethora of behavior [1], perhaps as exotic as the bulk properties themselves. A characterization of these excitations is motivated by several considerations. The spin excitations, which can be measured by a well understood and easily interpretable probe such as neutron scattering, provide a window on the electronic correlations in these complex materials. Indeed, Cooper pairing itself is a correlation between electron spins. A further motivation, especially in view of the unconventional pairing [2] in these materials, is that the magnetic excitations may be involved in the pairing attraction.

In the present paper we review our recent measurements [3–6] of the dynamic response over a wide frequency range i.e. up to energies of order 2J. We find that in the superconductors there is significant spectral weight above the superconducting gap energy. For both superconductors studied, the magnetic response $\chi''(q,\omega)$ is actually stronger for frequencies just above 2Δ than in the parent insulating antiferromagnet. We have been careful to convert our measurements into absolute units. This allows a systematic comparison between different systems, compositions and theories to be made.

II. EXPERIMENTAL

Our experiments were performed using the HET and MARI spectrometers at the ISIS pulsed spallation neutron source of the Rutherford Appleton Laboratory. HET and MARI are direct geometry chopper spectrometers. A pulse of neutrons of approximately 1 μ s duration is produced when a 800 MeV pulsed proton beam hits a tantalum target. The neutrons are monochromated using a Fermi chopper at 10 m from the target and appropriately phased to the proton pulse. Scattered neutrons are detected using 800 ³He detectors 4 m from the sample.

Neutron scattering directly measures the imaginary part of the generalized magnetic

susceptibility $\chi''(\mathbf{Q},\omega)$. The scattering cross-section for an isotropic system is [7],

$$\frac{d^2\sigma}{d\Omega dE} = (\gamma r_e)^2 \frac{k_f}{k_i} |F(\mathbf{Q})|^2 \left(\frac{2/\pi g^2 \mu_B^2}{1 - \exp(-\hbar\omega/kT)} \right) \chi''(\mathbf{Q}, \omega), \tag{1}$$

where $(\gamma r_e)^2$ =0.2905 barn sr⁻¹ μ_B^{-2} , \mathbf{k}_i and \mathbf{k}_f are the incident and final neutron wavevectors and $|F(\mathbf{Q})|^2$ is the magnetic form factor. Absolute unit conventions were performed by measuring the elastic incoherent scattering from a vanadium standard [8] under the same experimental conditions and by measuring the low-frequency coherent phonon scattering from the sample [9]. Throughout this paper, we label momentum transfers (Q_x, Q_y, Q_z) in units of Å⁻¹ by their reciprocal space positions \mathbf{Q} =(h, k, l)= $(2\pi Q_x/a, 2\pi Q_y/b, \pi Q_z/c)$. Following previous practice, we use the *orthorhombic* nomenclature to label reciprocal space in the $\mathrm{La}_{2-x}\mathrm{Sr}_x\mathrm{CuO}_4$ system and *tetragonal* nomenclature in the YBa₂Cu₃O_{6+x} system. This means that the CuO₂ planes are parallel to (010) in $\mathrm{La}_{2-x}\mathrm{Sr}_x\mathrm{CuO}_4$ and (001) in YBa₂Cu₃O_{6+x}. Details of the samples are given elsewhere [3–6]. In the case of the $\mathrm{La}_{2-x}\mathrm{Sr}_x\mathrm{CuO}_4$ system, data were collected with the (001) plane coincident with the principal scattering plane of the spectrometer. For YBa₂Cu₃O_{6+x}, the (1 $\overline{10}$) plane was used.

III. THE QUANTUM ANTIFERROMAGNETS

We first discuss the parent antiferromagnets La₂CuO₄ and YBa₂Cu₃O_{6.15}. For the purpose of this paper, we model the systems as a set of weakly coupled CuO₂ layers or bilayers. In this case, the high-frequency spin excitations can be described by the Heisenberg Hamiltonian for a single CuO₂ layer or bilayer,

$$H = \sum_{ij} J_{\parallel} \mathbf{S}_i \cdot \mathbf{S}_j + \sum_{ij'} J_{\perp} \mathbf{S}_i \cdot \mathbf{S}_{j'}.$$
 (2)

The first term in Eq. 2 represents the nearest-neighbor coupling between Cu spins in the same CuO₂ plane. The second term (not present in the single layer compound) represents the coupling between nearest-neighbor Cu spins in different layers.

In the case of the single layer compound $(J_{\perp} = 0)$, conventional spin-wave theory in the classical large-S limit yields the dynamic susceptibility

$$\chi''(\mathbf{Q},\omega) = Z_{\chi} \pi g^{2} \mu_{\mathrm{B}}^{2} S \left(\frac{1-\gamma(\mathbf{Q})}{1+\gamma(\mathbf{Q})}\right)^{1/2} \delta \left(\hbar\omega \pm \hbar\omega(\mathbf{Q})\right), \tag{3}$$

where,

$$\hbar\omega(\mathbf{Q}) = 2Z_c J_{\parallel} \left[1 - \gamma^2(\mathbf{Q}) \right]^{1/2},\tag{4}$$

and $\gamma(\mathbf{Q}) = \cos(\pi h)\cos(\pi l)$. We have included a "quantum renormalization" of the overall amplitude Z_{χ} . In the conventional linear spin-wave model applicable for large S, $Z_{\chi} = 1$. For small S, quantum corrections [10,11] become important (the Neel state is not a good approximation to the ground state) leading to a renormalization of the overall scale of the spin-wave dispersion and to a reduction in magnetic response with respect to the classical spin-wave theory. The renormalization of the overall scale can be included in the exchange constant $J^* = Z_c J$, where J is the exchange constant occurring in Eq. 2. The value of Z_{χ} can be obtained by neutron scattering, if measurements are placed on an absolute intensity scale. However, Z_c cannot be measured directly from neutron scattering and must be estimated from theory. In the case of the $S = \frac{1}{2}$ square-lattice antiferromagnet, Singh [10] and Igarashi [11] have estimated $Z_c = 1.18$ and $Z_{\chi} = 0.51$ based on a 1/S expansion.

The presence of the second term (i.e. $J_{\perp} \neq 0$) in Eq. 2 leads to the existence of two branches in the spin-wave dispersion which can be labeled according to whether neighboring spins in different planes rotate in the same direction ("acoustic" or "odd" mode) or in opposite directions ("optical" or "even" mode) about their time-averaged (ordered) directions. In the conventional linear spin-wave approximation, the acoustic and optic modes have the response functions [12]

$$\chi_{\rm op}''(\mathbf{Q},\omega) = Z_{\chi} \pi g^2 \mu_{\rm B}^2 S \left(\frac{1 - \gamma(\mathbf{Q}) + J_{\perp}/2J_{\parallel}}{1 + \gamma(\mathbf{Q})} \right)^{1/2}$$
 (5)

$$\times \sin^2 \left(\frac{\pi \, \Delta z \, l}{c} \right) \delta \left(\hbar \omega \pm \hbar \omega_{\rm op}(\mathbf{Q}) \right) \tag{6}$$

and

$$\chi_{\rm op}''(\mathbf{Q}, \omega) = Z_{\chi} \pi g^2 \mu_{\rm B}^2 S \left(\frac{1 - \gamma(\mathbf{Q})}{1 + \gamma(\mathbf{Q}) + J_{\perp}/2J_{\parallel}} \right)^{1/2}$$
 (7)

$$\times \cos^2\left(\frac{\pi \,\Delta z \,l}{c}\right) \delta\left(\hbar\omega \pm \hbar\omega_{\rm ac}(\mathbf{Q})\right),\tag{8}$$

respectively. The dispersion relations are

$$\hbar\omega_{\text{ac}}(\mathbf{Q}) = 2Z_c J_{\parallel} \left\{ 1 - \gamma^2(\mathbf{Q}) + J_{\perp}/J_{\parallel} \left[1 \pm \gamma(\mathbf{Q}) \right] \right\}^{1/2}, \tag{9}$$

where $\gamma(\mathbf{Q}) = \frac{1}{2}[\cos(2\pi h) + \cos(2\pi k)]$ and $\Delta z = 3.2$ Å is the separation of the CuO₂ planes in a bilayer. The inter-planar coupling term in Eq. 2 leads to no additional dispersion along the z-direction, only a modulation in the amplitude of the response which nevertheless can be used to distinguish between the two modes.

A. La₂CuO₄

The two-dimensionality of the scattering in La₂CuO₄ means that we are able to cut through the spin waves at several energy transfers for a single spectrometer setting. Fig. 1 shows data collected for E_i =300 meV and $\mathbf{k}_i \parallel (010)$ on the MARI spectrometer. Panels (b)-(f) show constant energy cuts along the (1,0,0) direction. A spin-wave peak is observed near h=1. Twin peaks due to spin waves propagating in opposite directions are not observed due to the poor out-of-plane resolution in the (001) direction. The broadening in the peak at higher frequencies is due to the spin-wave dispersion. A convenient way to display the data in Fig. 1 is as a local- or wavevector-integrated susceptibility $\chi''(\omega) = \int_{\rm BZ} \chi''(\mathbf{Q}, \omega) \, d^3 Q / \int d^3 Q$, this is shown in Fig. 2(a). The solid lines in Fig. 1(b)-(f) and Fig. 2 are fits to the spin-wave model described by Eq. 3. Quantitative analysis yields an exchange constant consistent with our previous determination [3] $J^* = 156 \pm 5$ meV and $Z_{\chi} = 0.39 \pm 0.1$. This is in agreement with the calculation of Igarashi [11] and demonstrates the importance of quantum corrections in this system.

B. $YBa_2Cu_3O_{6.15}$

As discussed above, the bilayer nature of this material results in two collective modes with additional structure to $\chi''(\mathbf{Q}, \omega)$ as compared with the single layer material. The optic mode

has a gap at the 2-D magnetic zone centers such as $(\frac{1}{2}\frac{1}{2}l)$ of $\hbar\omega_g=2\sqrt{J_{\perp}^*J_{\parallel}^*}$. Its intensity displays an overall modulation $\cos^2(\pi \Delta z l/c)$ which has maxima at positions $l = 0, 3.7, 7.3, \dots$ Correspondingly, the acoustic mode has an overall modulation of $\sin^2(\pi \Delta z \, l/c)$ and therefore has maxima at $l = 1.8, 5.5, \ldots$ We are able to probe the spin waves at various values of $\hbar\omega$ and l by varying the incident energy. Fig. 3(b)-(e) show data collected for different energy transfers at l values corresponding to positions where the scattering is predominately acoustic. As in La₂CuO₄, a peak is observed near the magnetic zone center, for all energy transfers investigated, due to propagating spin waves. Similar cuts probing l values where the optic mode dominates, are shown in Fig. 3(g)-(j). In this case, no peak is observed at the lowest energies because these energies are below the optic gap. A more convenient way to look at these data is in the form of a local susceptibility (see above). Fig. 4 shows the contributions of the two branches to the local susceptibility extracted from the data in Fig. 3. When the data are plotted in this way, we see that the optic and acoustic contributions are equal at higher frequencies. While below $\hbar\omega_g$, the contribution from the optical mode is zero within the experimental error. A detailed analysis [5] yields a value for the optic gap of $\hbar\omega_g = 74 \pm 5$ meV. A similar value for the optic gap was obtained using reactor-based instrumentation [13].

In order to determine the exchange constant J_{\perp}^* describing the coupling of spins in different planes, we also need to know J_{\parallel}^* because the optic gap is $\hbar\omega_g=2\sqrt{J_{\perp}^*J_{\parallel}^*}$. The inplane exchange coupling, J_{\parallel}^* can be obtained from a measurement of the high-frequency spin waves. Fig. 5 shows data collected with the higher incident energy E_i =600 meV. We note that for energy transfers above 245 meV there is little variation in the intensity, suggesting that this energy is close to the zone boundary energy. A simultaneous resolution-corrected fit of the linear spin wave model (Eqs. (5)-(7)) to all our data yields values for the exchange constants of $J_{\parallel}^* = 125 \pm 5$ meV and $J_{\perp}^* = 11 \pm 2$ meV. Further, since our measurements are in absolute units we are able to estimate the amplitude renormalization. We find a value of $Z_{\chi} = 0.4 \pm 0.1$, as for La₂CuO₄, again the quantum renormalization is close to the value

predicted by a 1/S expansion $(Z_{\chi} = 0.51)$.

IV. THE SUPERCONDUCTORS

Of particular interest is the nature of the spin fluctuations [14,4] for metallic and superconducting compositions. We have therefore studied the compounds La_{1.86}Sr_{0.14}CuO₄ (a composition close to optimal doping) and YBa₂Cu₃O_{6.6} (an underdoped superconductor). In both cases we find strong high-frequency spin fluctuations in the superconducting state.

A. $La_{1.86}Sr_{0.14}CuO_4$

Fig. 1(h)-(l) shows data collected for La_{1.86}Sr_{0.14}CuO₄ under the same conditions as Fig. 1 and in the *same units*. Doping has a dramatic effect on the magnetic excitations: at low frequencies, the peaks are broader in reciprocal space and at higher frequencies there is a large suppression of the intensity. At the highest frequencies, the peaks appear to be disappearing more rapidly in the superconductor than the insulator. This can be seen clearly when we extract and plot the local susceptibility in Fig. 2(b). When we include low frequency data from a reactor-based experiment, it becomes clear that the local response is peaked near 22 meV. Thus doping leads to a shift of spectral weight to intermediate energies.

B. $YBa_2Cu_3O_{6.6}$

The low frequency dynamics of superconducting YBa₂Cu₃O_{6+x} have been the subject of considerable investigation [1]. The YBa₂Cu₃O_{6.6}($T_c = 62.7 \text{ K}$) sample used in the current study is of high quality: it shows a sharp "resonance peak" [15] at 34 meV on entering the superconducting state and has recently been shown [16] to develop incommensurate peaks in $\chi''(\mathbf{q},\omega)$ for frequencies near 25 meV. We concentrate here on the nature of the dynamics for temperatures just above the superconducting transition temperature. Fig. 6 shows inelastic data collected for T = 80 K on the MARI spectrometer in a similar manner to that in Fig. 3.

The reader should note that the energies chosen for Fig. 6 are different from those chosen for Fig. 3 because of the different detector positions on the HET and MARI spectrometers. By assuming that the scattering has a Gaussian wavevector dependence for each energy, we have extracted the frequency variation of the acoustic and optical contributions to the local susceptibility $\chi''(\omega)$ from data such as those shown in the figure. Fig. 7 shows the results.

Comparison of Figs. 6 and 7 with Figs. 3 and 4 shows that the magnetic response has changed dramatically between the metal and the insulator. This is well-known at low frequencies [1], as in $La_{2-x}Sr_xCuO_4$, there is a large broadening of the low frequency peak in wavevector. More dramatic is the redistribution of spectral weight in energy revealed by the local susceptibility in Fig. 7. Inspection of Fig. 4 and Fig. 7, which are in the same units and therefore can be directly compared, shows that doping causes a shift of spectral weight from high frequencies (above 100 meV) into the range around 50-100 meV. The gap in the optic fluctuations remains and is possibly slightly reduced. Reactor-based measurements yield a similar value for the optic gap [17].

V. DISCUSSION

Our measurements of $\chi''(\omega)$ on La₂CuO₄ and YBa₂Cu₃O_{6.15} are summarized in Fig. 2(a) and Fig. 4. We note that observed $\chi''(\omega)$ for La₂CuO₄ and the acoustic branch of YBa₂Cu₃O_{6.15} are of approximately equal intensity: the units of the susceptibility are expressed per formula unit in both cases, YBa₂Cu₃O_{6+x} has two Cu in the CuO₂ planes per formula unit. When we compare our measurements on the quantum antiferromagnets La₂CuO₄ and YBa₂Cu₃O_{6.15}, we find that, in both cases, linear spin-wave theory accounts well for the dispersion and amplitude variation. However, an overall renormalization of the amplitude Z_{χ} must be included to account for the observed intensity of the one-magnon response. Our observations agree with calculations of Z_{χ} =0.51 based on a 1/S expansion. Although we are able to explain the one-magnon excitation spectrum, the 1/S expansion also predicts additional spectral weight [11] which has not yet been observed.

We now turn the metals $La_{1.86}Sr_{0.14}CuO_4$ and $YBa_2Cu_3O_{6.6}$. The response of the copper spins obeys the sum rule,

$$\left\langle m^2 \right\rangle = \frac{3\hbar}{\pi} \int_{-\infty}^{\infty} \frac{\chi''(\omega) \, d\omega}{1 - \exp(-\hbar\omega/kT)}$$
 (10)

where $\langle m^2 \rangle$ is the mean squared moment on the Cu sites. In both superconductors studied here, doping and the consequential metal-insulator transition led to a large redistribution of spectral weight and formation of a peak in $\chi''(\omega)$ at intermediate frequency. In the light of the sum rule, the existence of the peak in itself is not unexpected since spectral weight is lost from the Bragg peak present in the insulator and the high frequency response is strongly suppressed. What is surprising is the relatively small energy scale over which the response is distributed compared with other paramagnetic metals. Such small electronic energy scales are, of course, characteristic of the cuprate superconductors.

Work at ORNL is supported by US-DOE under Contract No. DE-AC05-96OR22464 with Lockheed Martin Research, Inc. We are grateful for the finacial support of the UK-EPSRC and NATO.

REFERENCES

- See e.g. J. M. Tranquada, et al., Phys. Rev. Lett. 60, 156 (1988); J. Rossat-Mignot, et al., Physica 185-189, 86 (1991); H. A. Mook et al., Phys. Rev. Lett. 70, 3490 (1993);
 H. F. Fong et al., Phys. Rev. Lett. 75, 316 (1995).
- [2] D. J. Scalapino, Phys. Rep. **250**, 329 (1995).
- [3] G. Aeppli et al., Phys. Rev. Lett. 62 2052 (1989); S. M. Hayden et al., Phys. Rev. Lett. 67, 3622 (1991).
- [4] S. M. Hayden *et al.*, Phys. Rev. Lett. **76**, 1344 (1996).
- [5] S. M. Hayden et al., Bull. Am. Phys. Soc. 41, 400 (1996); S. M. Hayden et al., Phys. Rev. B 54, R6905 (1996).
- [6] P. Dai et al., unpublished.
- [7] See, e.g. R. M. White, *Quantum Theory of Magnetism*, Springer Ser. Solid-State Sci., Vol. 32 (Springer, Berlin 1983) ch 8. Throughout this paper we use the reduced susceptibility as discussed in this reference.
- [8] C. G. Windsor, Pulsed Neutron Scattering (Taylor and Francis, London, 1981).
- [9] 0. Steinsvoll *et al.*, Phys. Rev. B **30**, 2377 (1984).
- [10] R. R. P. Singh, Phys. Rev. B **39**, 9760 (1989).
- [11] J. Igarashi, Phys. Rev. B 46, 10763 (1992); J. Phys.: Condens. Matter 4, 10265 (1992).
- [12] J. M. Tranquada, Phys. Rev. B **40** 4503 (1989).
- [13] D. Reznik *et al.*, Phys. Rev. B **53**, R14741. (1996).
- [14] K. Yamada et al., J. Phys. Soc. Jpn. **64**, 2742 (1995).
- [15] P. Dai et al., Phys. Rev. Lett. 77, 5425 (1996).

- [16] P. Dai $et\ al.,$ preprint cond-mat/9707112
- [17] P. Bourges et al., preprint cond-mat/970473
- [18] G. Aeppli et al., to be published in Science.

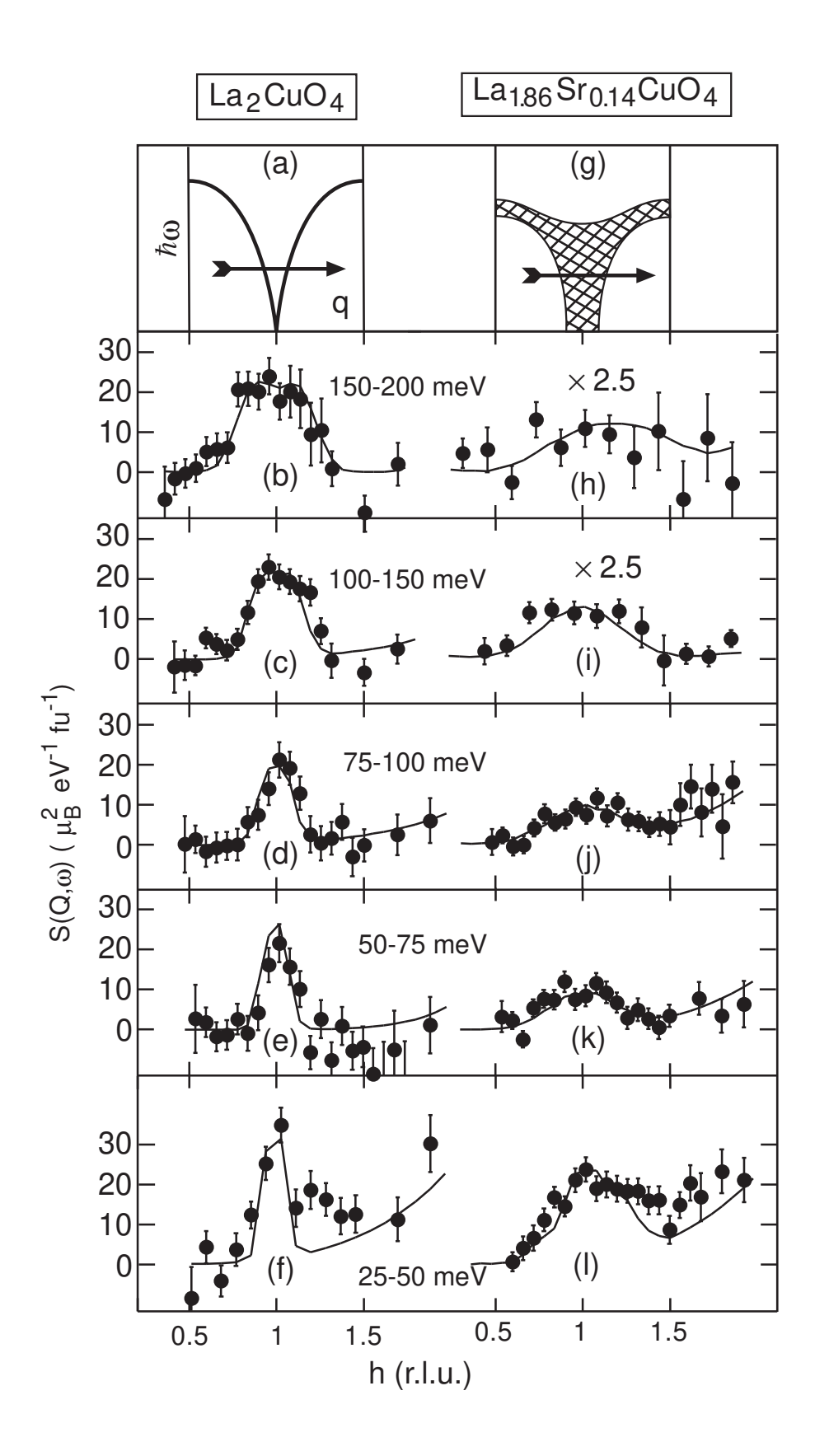
FIGURES

- FIG. 1. (a)-(f) Magnetic scattering from La₂CuO₄ and (g)-(l) from La_{1.86}Sr_{0.14}CuO₄ [4]. All scans are in the same absolute units. Note the magnetic peak is broader in the superconductor and suppressed at higher frequencies.
- FIG. 2. Local susceptibility [4] derived from data such as that in Fig. 1 (closed circles) and from reactor-based measurements [18]. Note huge redistribution of spectral weight caused by doping.
- FIG. 3. Constant energy scans showing magnetic scattering from YBa₂Cu₃O_{6.15} for wavevectors $\mathbf{Q} = (h, h, l)$. (b)-(e) l chosen to emphasize acoustic modes. (g)-(j) l chosen to emphasize optic modes. The onset of scattering at the optic position is about 74 meV.
- FIG. 4. Local or wavevector-integrated energy-dependent magnetic susceptibility at acoustic and optic l-positions in YBa₂Cu₃O_{6.15}. No integration over l has been performed. Points have been obtained by integrating over the spin-wave peaks and correcting for the Cu²⁺ magnetic form factor, Bose factor and instrumental resolution. Solid lines are a fit to the spin wave model described in the text.
- FIG. 5. (a) Dispersion relation of YBa₂Cu₃O_{6.15}. Closed circles and solid line are acoustic mode. Open circles and dashed line are optic mode. (b)-(e) Constant energy scans showing the high-frequency magnetic scattering from YBa₂Cu₃O_{6.15}.
- FIG. 6. Constant energy scans showing magnetic scattering from YBa₂Cu₃O_{6.6} for wavevectors $\mathbf{Q} = (h, h, l)$. (a)-(c) l chosen to emphasize acoustic modes. (d)-(f) l chosen to emphasize optic modes.
- FIG. 7. Acoustic and optic contributions to the local susceptibility (see Fig. 4) in YBa₂Cu₃O_{6.6}. Solid lines are a guide to the eye.

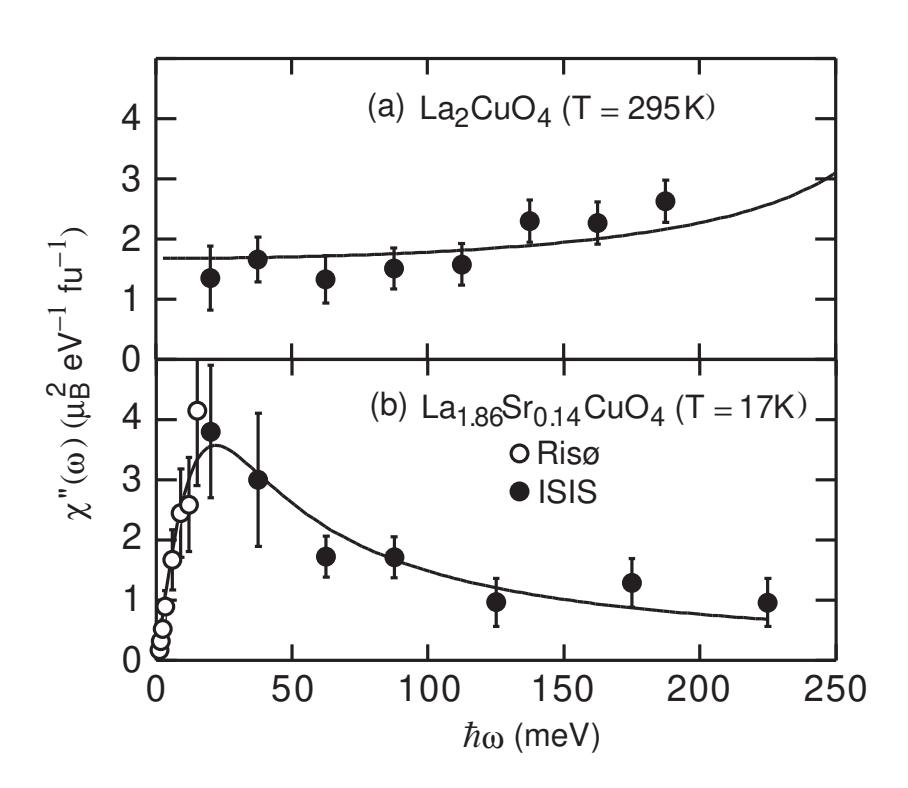
TABLES

TABLE I. The table summarizes experimentally-determined spin-wave parameters for $\text{La}_{2-x}\text{Sr}_x\text{CuO}_4$ and $\text{YBa}_2\text{Cu}_3\text{O}_{6+x}$. In the case of the superconductors, J_{\parallel}^* and Z_c are determined from the highest frequencies studied.

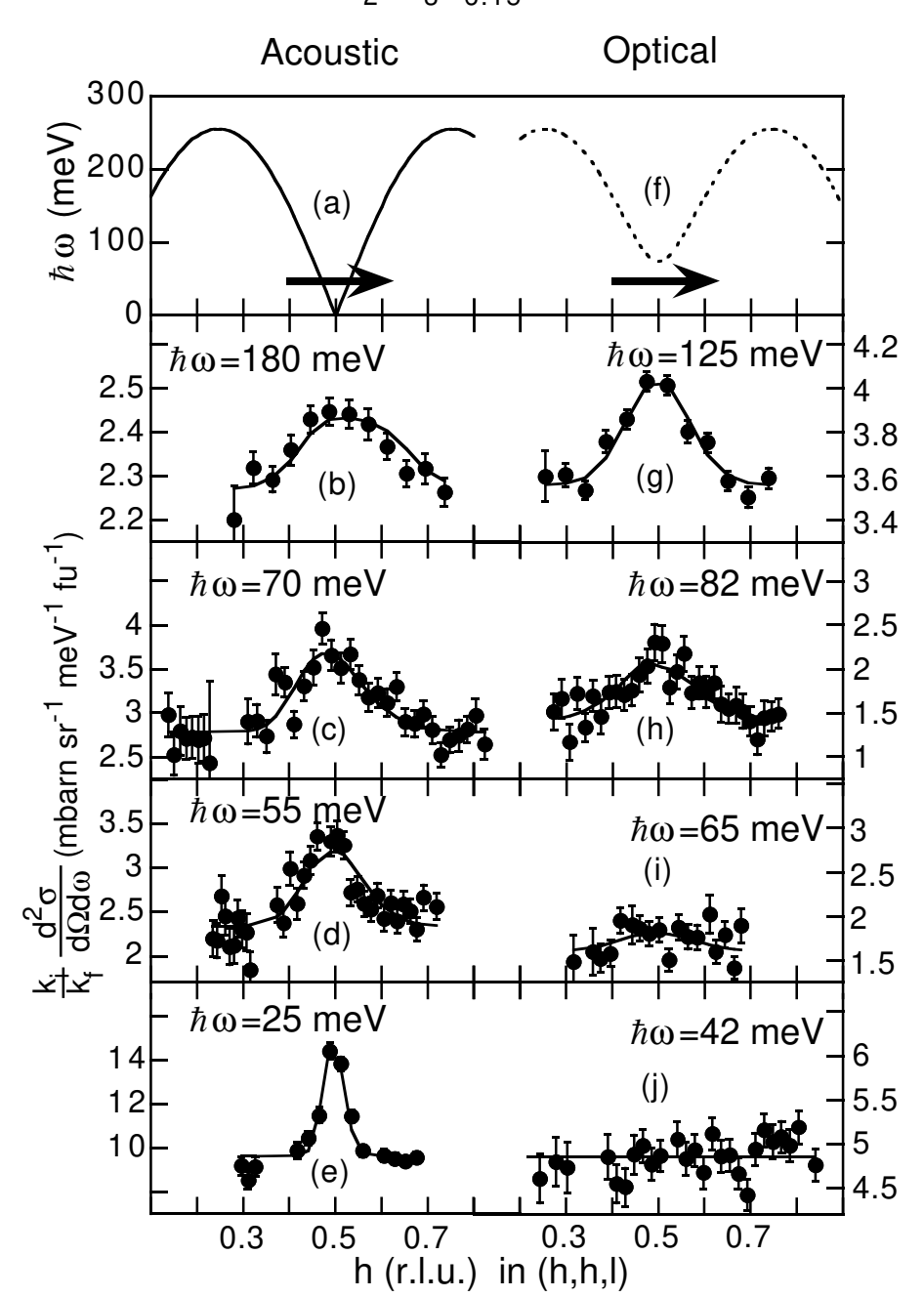
	J_{\parallel}^{*}	J_{\perp}^{*}	Z_χ	$\hbar\omega_g$
La ₂ CuO ₄	$156 \pm 5~\mathrm{meV}$		0.39 ± 0.1	
$\rm La_{1.86}Sr_{0.14}CuO_4$	$130 \pm 5~\mathrm{meV}$		0.15 ± 0.06	
$YBa_{2}Cu_{3}O_{6.15}$	$125 \pm 5~\mathrm{meV}$	$11 \pm 2 \mathrm{meV}$	0.4 ± 0.1	$74 \pm 5 \text{ meV}$
YBa ₂ Cu ₃ O _{6.6}	${\sim}120~\mathrm{meV}$			$\sim 60~\mathrm{meV}$



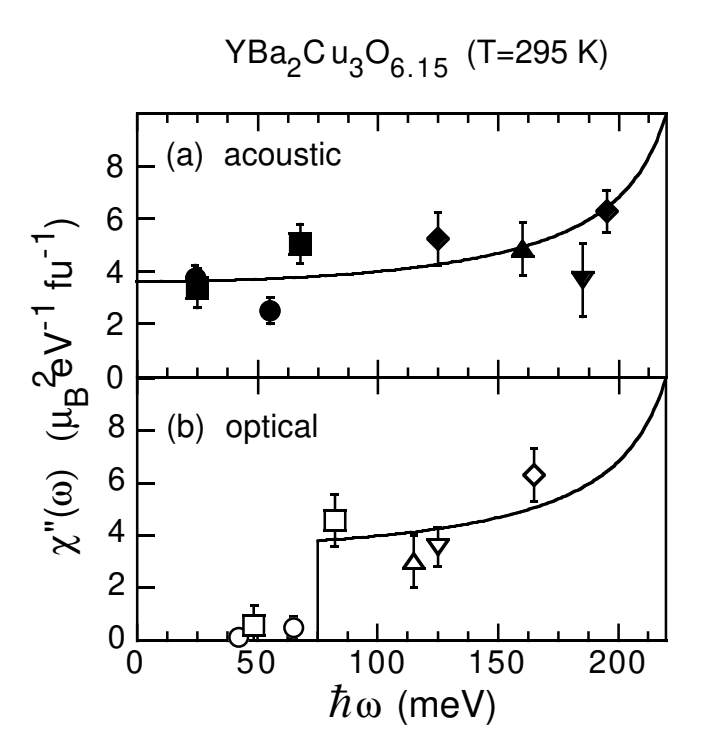
Hayden et al Fig. 1



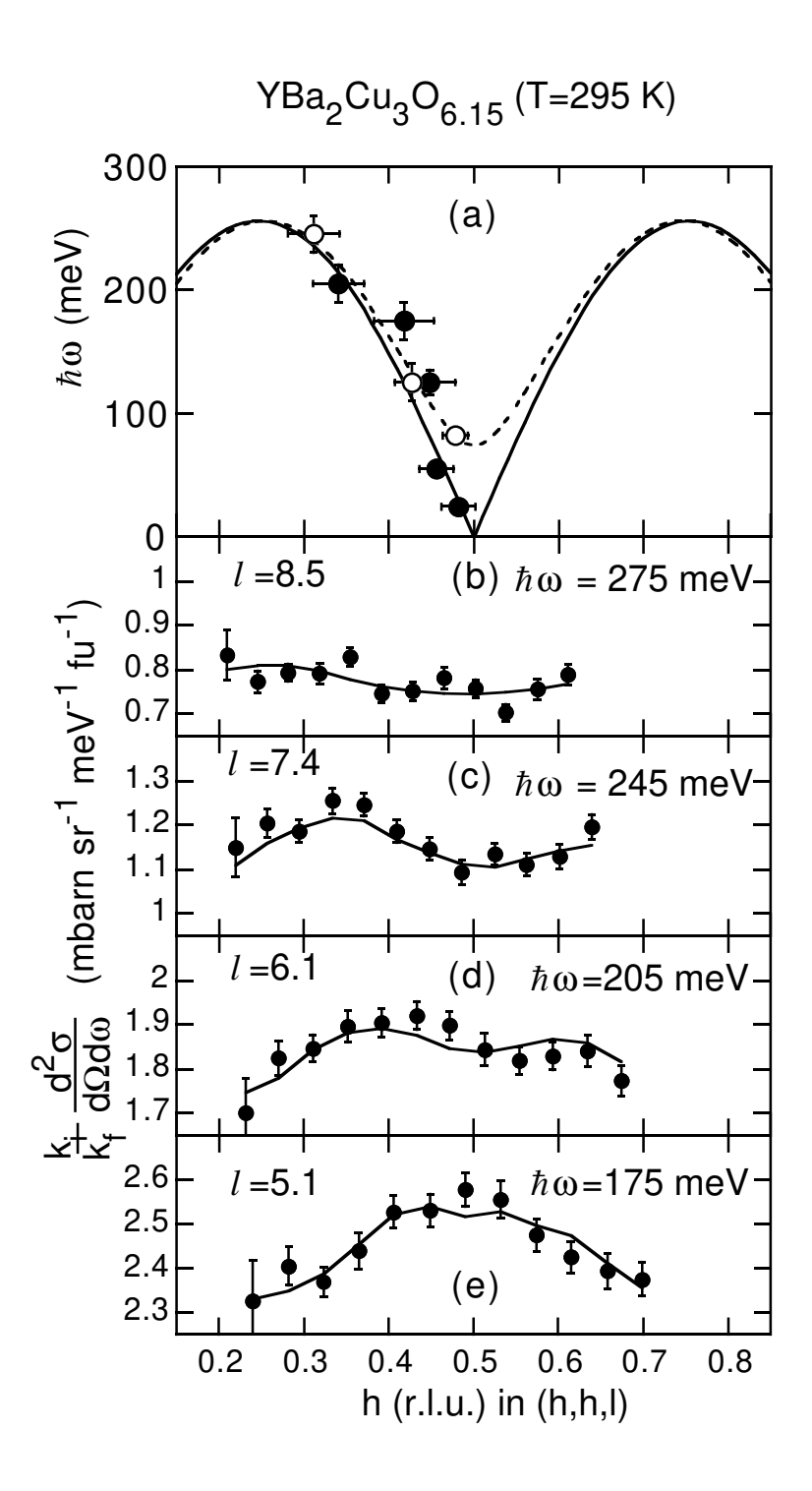
$YBa_{2}Cu_{3}O_{6.15}$ (T=295 K)



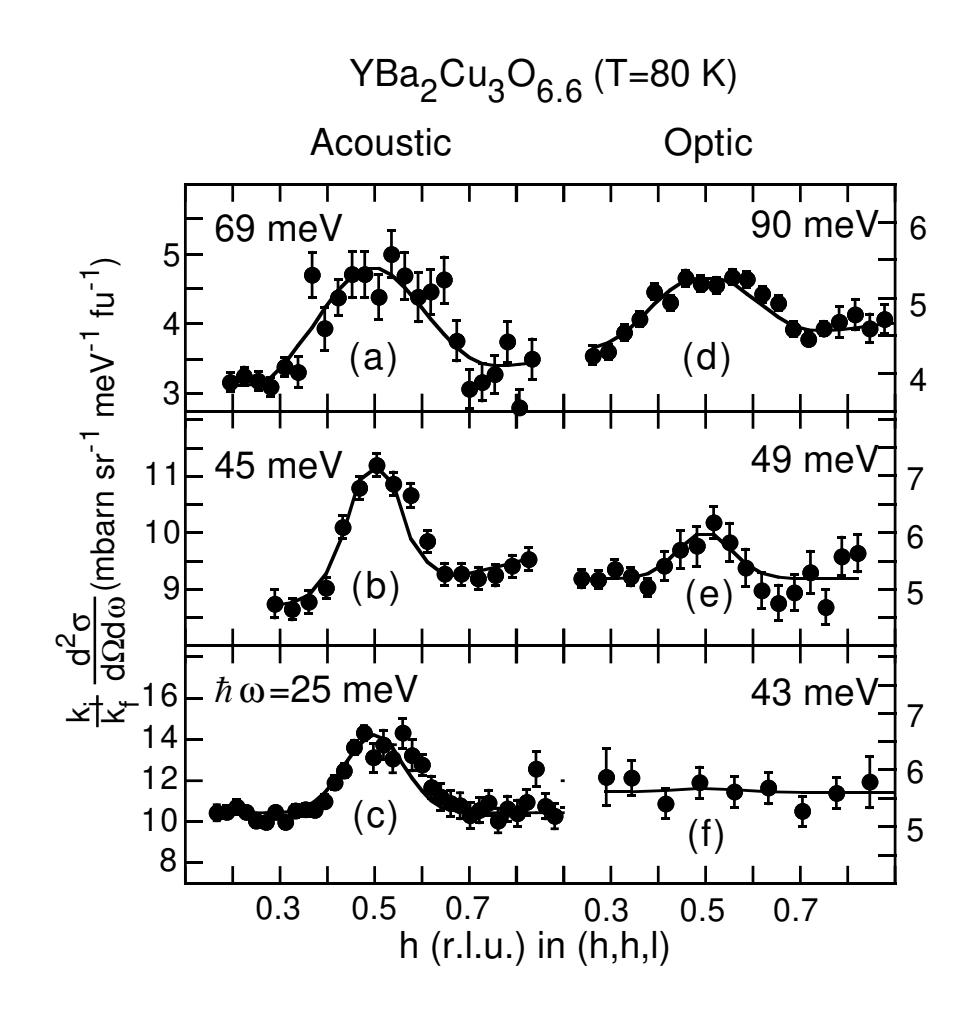
Hayden et al. Fig. 3

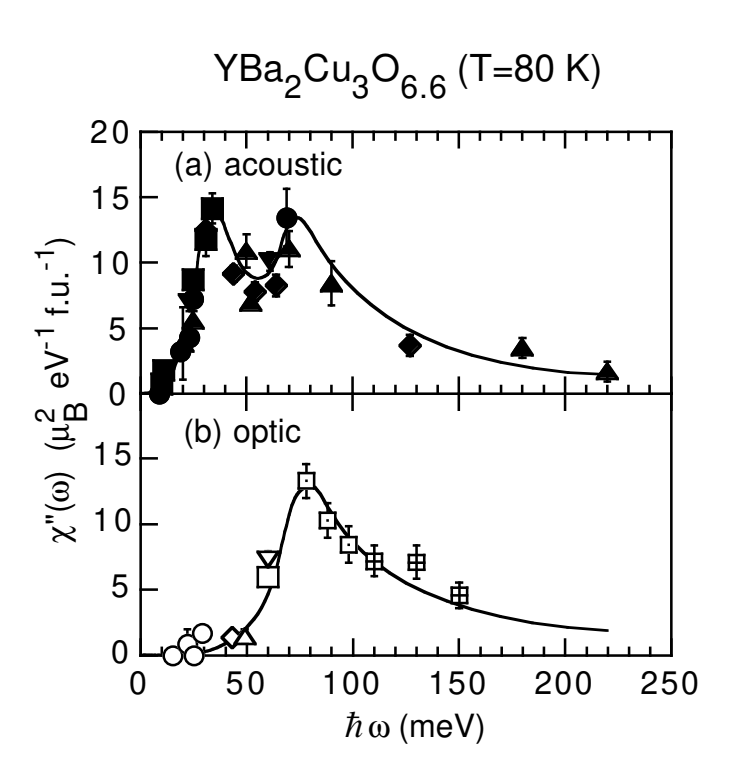


Hayden et al. Fig. 4



Hayden et al. Fig. 5





Hayden et al. Fig. 7